X-ray dynamical diffraction from multilayer Laue lenses with rough interfaces

Hanfei Yan

National Synchrotron Light Source II, Brookhaven National Laboratory, Upton, New York 11973, USA

(Received 26 November 2008; revised manuscript received 17 February 2009; published 8 April 2009)

A modeling approach for x-ray dynamical diffraction from multilayer Laue lenses (MLLs) with rough interfaces is developed. Although still based on the principle of the distorted-wave Born approximation (DWBA), this model is formulated from the perspective of the physical scattering process, very different from the conventional DWBA formalism. Using this model, one can study x-ray scattering from rough interfaces in the regime of Fresnel diffraction and in the case of absorptive samples, for example, x-ray dynamical diffraction from MLLs with rough interfaces, which is hard to handle in the framework of the conventional DWBA. Theoretical simulations for various MLLs with rough interfaces are conducted. It is found that interfacial roughness results in a decrease in the local diffraction intensity, where the attenuation factor is a function of the root-mean-square (rms) roughness versus the local zone width ratio. This study shows that if all zones possess an identical rms roughness value that is less than half of the outmost MLL zone width, the focal broadening effect due to roughness is almost unnoticeable, provided that the mean position of the interface does not deviate from the required zone plate law. A further study shows that uncorrelated interfacial roughness can be treated the same as interfacial diffusion, in which case a roughness factor similar to the "Debye-Waller factor" can be used, and the pseudo-Fourier coefficients of the susceptibility function for an MLL [H. F. Yan *et al.*, Phys. Rev. B **76**, 115438 (2007)] have to be multiplied by this factor.

DOI: 10.1103/PhysRevB.79.165410 PACS number(s): 61.05.cc, 41.50.+h, 68.35.Ct, 07.85.Qe

I. INTRODUCTION

Recent progress in x-ray focusing optics has pushed the frontier of x-ray microscopy into the 25–50 nm range.[1–7] However, because of the small refraction power of materials for x rays, many of these x-ray optics possess a lower focal limit of about 10 nm.[8–10] In order to overcome this limit and achieve true nanometer-scale resolution, a novel diffractive focusing optic called a multilayer Laue lens (MLL) has been proposed and developed.[1,11,12] To date, a line focus of 16 nm has been achieved by MLL optics at energy of 19.5 keV.[13] Theoretical studies indicate that MLL optics are capable of achieving subnanometer foci when ideal structures without imperfections such as zone placement error or interface diffusion and roughness are used.[14] Unfortunately, imperfections always exist in real optics and will degrade their performance. For example, a small zone placement error in an MLL can significantly broaden its focal size and introduce strong undesirable background.[15] Interface roughness is another common type of imperfection in MLL optics, and its importance increases as zone width decreases. According to the Rayleigh criterion and the zone plate law, the focus size of an MLL is scaled with its outmost zone width. For example, in order to achieve 1-nm focus one has to fabricate an MLL with 1-nm outmost zone width, which is composed of just a few monolayers and the interface is rough on the atomic scale. It is thereby critically important to understand the magnitude and extent of the adverse effect of interface roughness on MLL's focusing performance.

There have been some prior theoretical works investigating the effects of interface roughness on zone plate performance,[16,17] but these studies were rather limited and were restricted to a local region. On the other hand, the distorted-wave Born approximation (DWBA) is widely applied in studying x-ray scattering from single or multiple rough interfaces.[18–23] DWBA yields an integral solution that is well suited for carrying out a statistical average, and enables one to study not only the coherent but also the incoherent (diffuse) scattering. The conventional DWBA formalism, which stems from the two-potential formula in quantum mechanics,[24] utilizes the time-inverted solution as an eigenfunction to calculate the scattering matrix.[19] The mathematical basis of this formalism is built on the fact that the Green's function for the unperturbed system (no roughness) can be approximated as the time-inverted solution when (1) the observation point is located at infinity (Fraunhoffer diffraction) and (2) absorption is negligible so that the reciprocity theorem holds.[25] However both conditions are not satisfied for MLLs. The wave propagation after an MLL to its focal plane falls into the regime of Fresnel diffraction and because of the large section depth required to achieve high efficiency, the photoelectric absorption inside an MLL cannot be ignored. As a result the conventional DWBA formalism is inapplicable here. Nevertheless the principle of DWBA, splitting the perturbed system into an unperturbed one and small perturbations, can be borrowed.

The aim of this paper is twofold: develop a modeling approach for x-ray scattering from rough interfaces that is not limited by the above two conditions, and apply it to investigate the focusing performance of MLLs with rough interfaces. This model is still based on the principle of DWBA, but is formulated from the physical picture of the scattering process. Without the need for applying Green's theorem, the difficulty of finding the proper Green's function is avoided. This model also yields an integral solution suitable for ensemble averaging. Moreover, by taking into account high-order corrections this modeling approach is extended to deal with a strong perturbation, which is the case when interface roughness becomes comparable to the zone width. Theoretical simulations show that stochastic roughness results in a decrease in the local diffraction intensity.

The attenuation factor turns out to be a function of the $\sigma/\Delta x$ ratio, where σ and Δx are the rms roughness and the local zone width, respectively. It is found that when the ratio of $\sigma/\Delta x_{\min}$ is less than 0.5, where $\Delta x_{\min}$ is the outermost zone width, an MLL suffers only a loss in the focusing efficiency; the focal size is nearly unchanged. However, this broadening effect on the focus size becomes more noticeable as this ratio is increased to above 0.5, in which case the local diffraction intensity in the outer part of the MLL is attenuated to nearly zero. This leads to a reduction in the effective numerical aperture since the outer part does not contribute to focusing anymore.

A further study shows that uncorrelated roughness can be treated equivalently to an interdiffusion problem for MLLs. In such cases, one simply needs to use a roughness factor similar to the "Debye-Waller factor," $\exp(-M_h) = \langle \exp(i\boldsymbol{\rho}_{\mathbf{h}} \cdot \mathbf{u}) \rangle$, where $\boldsymbol{\rho}_{\mathbf{h}}$ is the hth local reciprocal-lattice vector, $\mathbf{u}$ is the random displacement vector of the interface, and the angle bracket denotes the statistical average. The pseudo-Fourier coefficients of the susceptibility function for an MLL (Ref. 14) have to be multiplied by this factor to account for the effect of roughness.

II. THEORETICAL MODELING

The electric wave field inside an MLL obeys the scalar wave equation

$$\nabla^2 E(\mathbf{r}) + k^2[1 + \chi(\mathbf{r})]E(\mathbf{r}) = 0, \tag{1}$$

where $k = 2\pi/\lambda$, λ is the wavelength of the incoming x ray, and $\chi(\mathbf{r})$ is the susceptibility function of the MLL. Splitting $\chi(\mathbf{r})$ into two parts provides

$$\chi(\mathbf{r}) = \bar{\chi}(\mathbf{r}) + \delta\chi(\mathbf{r}), \tag{2}$$

where $\bar{\chi}(\mathbf{r})$ is the susceptibility function for the MLL with flat interfaces (no roughness) and $\delta\chi(\mathbf{r})$ represents the fluctuation of $\chi(\mathbf{r})$ caused by interface roughness. $\delta\chi(\mathbf{r})$ is nonzero only in the vicinity of the interface. Similarly, the solution to Eq. (1) may be written as two parts as well,

$$E(\mathbf{r}) = \bar{E}(\mathbf{r}) + \delta E(\mathbf{r}), \tag{3}$$

in which

$$\nabla^2 \bar{E}(\mathbf{r}) + k^2[1 + \bar{\chi}(\mathbf{r})]\bar{E}(\mathbf{r}) = 0, \tag{4a}$$

$$\nabla^2 \delta E(\mathbf{r}) + k^2[1 + \bar{\chi}(\mathbf{r})]\delta E(\mathbf{r}) = -k^2 \delta\chi(\mathbf{r}) E(\mathbf{r}). \tag{4b}$$

For given boundary conditions, the solution to Eq. (4a), $\bar{E}(\mathbf{r})$ (denoted as the reference wave hereafter), can be obtained using the approach developed previously.[14] The solution to Eq. (4b), $\delta E(\mathbf{r})$, which corresponds to the additional fluctuating wave induced by roughness, can be written as an integral equation by Green's theorem,

$$\delta E(\mathbf{r}) = k^2 \int_V G(\mathbf{r};\mathbf{r}')\delta\chi(\mathbf{r}')E(\mathbf{r}')d^3\mathbf{r}', \tag{5}$$

where V is the whole volume of the MLL and $G(\mathbf{r};\mathbf{r}')$ is the Green's function satisfying

$$\nabla^2 G(\mathbf{r};\mathbf{r}') + k^2[1 + \bar{\chi}(\mathbf{r})]G(\mathbf{r};\mathbf{r}') = -\delta(\mathbf{r} - \mathbf{r}'). \tag{6}$$

So far no approximations have been made and the solution in Eq. (5) is rigorous. In cases with weak scattering from roughness, $|\delta E| \ll |\bar{E}|$, as the first-order approximation, Eq. (5) can be approximated to

$$\delta E(\mathbf{r}) \approx k^2 \int_V G(\mathbf{r};\mathbf{r}')\delta\chi(\mathbf{r}')\bar{E}(\mathbf{r}')d^3\mathbf{r}'. \tag{7}$$

This is the well-known first-order DWBA and has been proved to be very powerful in the study of x-ray scattering by rough interfaces. A great advantage of this formalism is that the expression of the solution is ready for carrying out a statistical average on the fluctuating wave. Solving Eq. (7) boils down to finding the proper Green's function in Eq. (6), which is usually cast into the form of the time-inverted solution to Eq. (4a) under the following conditions: (1) the observation point is at infinity and (2) there is no absorption. However, both of them are invalid for the wave field calculation around the focus of a thick absorbing MLL. Consequently, standard procedures of calculating the fluctuating wave in the conventional DWBA cannot be applied here. Instead, by considering a physical picture of the scattering process we present a modeling approach that does not have these limitations.

The physical picture described by Eq. (4b) comprises four scattering processes:

(1) The first term on the right-hand side, $k^2\delta\chi\bar{E}$, represents the scattering of the reference wave by roughness, and is the internal source of the fluctuating wave.

(2) Terms on the left-hand side describe the propagation and diffraction of the fluctuating wave, δE, inside the MLL in the absence of roughness.

(3) The second term on the right-hand side of Eq. (4b), $k^2\delta\chi\delta E$, represents the scattering of the fluctuating wave by roughness and is a high-order scattering process.

(4) Processes 2 and 3 change the value of δE generated in process 1 as it propagates through the MLL, forming a self-consistent system.

Applying the first-order DWBA is equivalent to ignoring the last two processes, so that it becomes very straightforward to calculate the fluctuating wave. The central idea here is to divide the MLL into many segments with progressively reduced section depth. Each segment consists of a very thin slice of MLL with rough interfaces upfront and an MLL with flat interfaces and section depth $t - z'$ (Fig. 1), where t is the section depth of the whole MLL. The fluctuating wave is first excited inside the very thin slice at z' (process 1) and then propagates through the MLL with flat interfaces to its exit surface (process 2), during which dynamical diffraction is taken into account. Consequently, the total fluctuating wave on the exit surface of the MLL is the summation of contributions from all segments,

$$\delta E(\mathbf{r}_\mathbf{e}) = \int_0^t dz' \int\int_\Omega p_{z'}(\mathbf{r};\mathbf{r}_\mathbf{e}) s_{z'}(\mathbf{r}) dxdy, \tag{8}$$

where $s_{z'}(\mathbf{r})$ is the source fluctuating wave generated in the thin slice at z', $\mathbf{r}_\mathbf{e}$ is a point on the exit surface, Ω is the

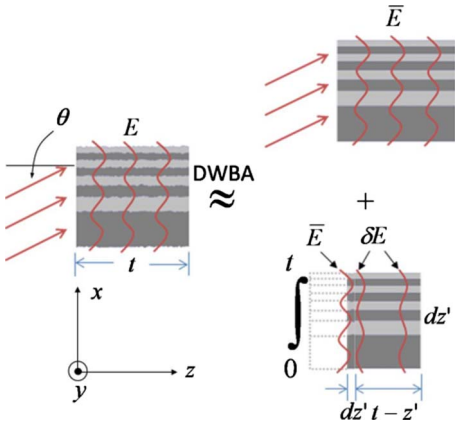

FIG. 1. (Color online) Schematic of an incident plane wave diffracted by an MLL with rough interfaces. Based on the principle of DWBA, the perturbed system (graph on the left) is split into an unperturbed one (top graph on the right) and perturbations (bottom graph on the right). The interaction between the fluctuating wave and roughness is neglected in this drawing.

cross-sectional area of the MLL, and $p_{z'}(\mathbf{r};\mathbf{r_e})$ is the propagator that describes the propagation of the fluctuating wave generated at z' from $\mathbf{r}$ to $\mathbf{r_e}$. If the slice is sufficiently thin, the scattering process within it is kinematical and the source fluctuating wave can be calculated using Born's approximation (BA),

$$s_{z'}(\mathbf{r}) = \int\int G_0(\mathbf{r};\mathbf{r}')\delta\chi(\mathbf{r}')\bar{E}(\mathbf{r}')dx'dy' \tag{9}$$

where $G_0(\mathbf{r};\mathbf{r}')$ is the free space Green's function satisfying

$$\nabla^2 G_0(\mathbf{r};\mathbf{r}') + k^2 G_0(\mathbf{r};\mathbf{r}') = -\delta(\mathbf{r}-\mathbf{r}'). \tag{10}$$

This is the key approximation made in this model. Speaking rigorously, the Green's function satisfying Eq. (6) should be used in calculating the source fluctuating wave in Eq. (9), but because the value of $\bar{\chi}$ is very small ($\sim 10^{-5}$), the interaction between δE and $\bar{\chi}$ can be neglected as dz' goes to zero. One shall note that this approximation is only valid inside the very thin slice. The propagation and diffraction of the fluctuating wave in the rest of the MLL afterwards have to be calculated by a dynamical model.

For convenience, G_0 is expressed in reciprocal space,

$$G_0(\mathbf{r};\mathbf{r}') = \frac{i}{8\pi^2}\int\int_{-\infty}^{\infty}\frac{1}{k_z}\exp[i\mathbf{k}\cdot(\mathbf{r}-\mathbf{r}')]dk_x dk_y,$$
$$k_z = \sqrt{k^2 - k_x^2 - k_y^2}. \tag{11}$$

Because only the forward propagating waves are concerned, k_z is taken positive. Substituting Eq. (11) into Eq. (9), one arrives at

$$s_{z'}(\mathbf{r}) = \frac{ik^2}{8\pi^2}\int\int_{-\infty}^{\infty}\frac{1}{k_z}\exp(i\mathbf{k}\cdot\mathbf{r})dk_x dk_y \int\int \times\exp(-i\mathbf{k}\cdot\mathbf{r}')\delta\chi(\mathbf{r}')\bar{E}(\mathbf{r}')dx'dy'. \tag{12}$$

Since an MLL is a one-dimensional (1D) focusing optic, here it is assumed that the system is independent of y. After integrating out the y dimension, which results in a 2π constant, the fluctuating wave generated at z' can be written as a superposition of many plane waves,

$$s_{z'}(\mathbf{r}) = \int S_{z'}(\mathbf{k})\exp(i\mathbf{k}\cdot\mathbf{r})dk_x,$$
$$S_{z'}(\mathbf{k}) = \frac{ik^2}{4\pi k_z}\int \exp(-i\mathbf{k}\cdot\mathbf{r}')\delta\chi(\mathbf{r}')\bar{E}(\mathbf{r}')dx',$$
$$k_z = \sqrt{k^2 - k_x^2}. \tag{13}$$

From now on we assume that all vectors have only x and z components.

If only the wave field near the focus (which is mainly contributed from plane waves with wave vectors $\mathbf{k}\approx\mathbf{k_0}$) is of interest, we have the approximation $k_z \approx k\cos\theta$, where θ is the tilting angle and $\mathbf{k_0}$ is the wave vector of the incident plane wave (see Fig. 1). Then right after the slice ($z=z'$), the source fluctuating wave can be written as

$$s_{z'}(\mathbf{r}) = \frac{ik^2}{4\pi}\int\frac{dk_x}{k_z}\int\exp[i\mathbf{k}\cdot(\mathbf{r}-\mathbf{r}')]\delta\chi(\mathbf{r}')\bar{E}(\mathbf{r}')dx'$$
$$\approx \frac{ik}{2\cos\theta}\delta\chi(\mathbf{r})\bar{E}(\mathbf{r}), \quad \mathbf{r} = (x,z'). \tag{14}$$

This is simply the fluctuation of the susceptibility function at z' multiplied by the reference wave at the same position and some constants. Not surprisingly, this is what the geometrical-optical theory predicts. Now if the propagator $p_{z'}(\mathbf{r};\mathbf{r_e})$ is known, one can calculate the total fluctuating wave on the exit surface.

It is known that for an incident plane wave $\exp(i\mathbf{k_0}\cdot\mathbf{r})$, the reference wave $\bar{E}(\mathbf{r})$ can be expressed as a superposition of many orders of diffracted waves which converge to the real foci (or diverge from the virtual foci) of an MLL,[14]

$$\bar{E}(\mathbf{r}) = \exp(i\mathbf{k_0}\cdot\mathbf{r})\sum_h \bar{E}_h(\mathbf{r})\exp[i\phi_h(\mathbf{r})]. \tag{15}$$

For simplicity, here an MLL with flat zones that follow the simplified zone plate law is assumed; so one has

$$\phi_h = \frac{h\pi}{\lambda f}x^2. \tag{16}$$

It is not difficult to extend this study to other types of MLLs. Substituting Eq. (15) into Eq. (14), one arrives at

$$s_{z'}(\mathbf{r}) = \frac{ik}{2\cos\theta}\exp(i\mathbf{k_0}\cdot\mathbf{r})\delta\chi(\mathbf{r})\sum_h \bar{E}_h(\mathbf{r})\exp[i\phi_h(x)]. \tag{17}$$

For an MLL consisting of many alternating layers A and B, if $u_j(z)$ is the displacement function of the jth rough interface along the x axis from its mean position, $\delta\chi$ can be expressed as

$$\delta\chi = \sum_j \delta\chi_j = \Delta\chi\sum_j (-1)^j U_j,$$

$$U_j = \begin{cases} 1, & \text{for } 0 < x - x_j < u_j(z) \quad \text{if } u_j(z) > 0 \\ -1, & \text{for } u_j(z) < x - x_j < 0 \quad \text{if } u_j(z) < 0 \\ 0, & \text{elsewhere,} \end{cases}$$

$$\Delta\chi = \chi_B - \chi_A, \tag{18}$$

where $x_j = \sqrt{j\lambda f}$ is the mean position of the jth interface. As can be seen from Eq. (18), although u_j varies randomly, the overall positioning of $\delta\chi$ still follows the zone plate law because $\delta\chi$ is nonzero only at positions around x_j. Based on this observation one can postulate that the source fluctuating wave $s_{z'}(\mathbf{r})$ can be expanded into a similar series as in Eq. (15),

$$s_{z'}(\mathbf{r}) = \exp(i\mathbf{k_0}\cdot\mathbf{r})\sum_l A_{z',l}(x)\exp[i\phi_l(x)]. \tag{19}$$

In order to obtain the correct form of $A_{z',l}$, we follow similar procedures of deriving pseudo-Fourier series in Ref. 14. Defining a different variable,

$$X = \mathrm{sgn}(x)x^2, \quad \mathrm{sgn}(x) = \begin{cases} 1, & x > 0 \\ 0, & x = 0 \\ -1, & x < 0. \end{cases} \tag{20}$$

In this way x is mapped to X point by point. As a result, one has (for the MLL half on the positive x axis)

$$X_j = x_j^2 = j\lambda f.$$

After this variable transform, the MLL becomes a periodic grating with a period of $2\lambda f$. Following this, one can perform a Fourier transform with respect to X on the source fluctuating wave [Eq. (17)] written as

$$s_{z'}(\mathbf{r}) = \exp(i\mathbf{k_0}\cdot\mathbf{r})\int_{-\infty}^{\infty}\Phi_{z'}(\varphi)\exp(i\varphi X)d\varphi, \tag{21}$$

where

$$\begin{aligned}\Phi_{z'}(\varphi) &= \frac{1}{2\pi}\int_{-\infty}^{\infty}\frac{ik}{2\cos\theta}\delta\chi(X,z')\sum_h \bar{E}_h(X,z')\exp(-i\varphi X)dX \\ &= \frac{ik}{4\pi\cos\theta}\sum_h\sum_j(-1)^j\Delta\chi\int_{x_j}^{x_j+u_j}\bar{E}_h(x,z') \\ &\quad\times\exp[i\phi_h(x) - i\varphi x^2]dx^2.\end{aligned} \tag{22}$$

Because $\bar{E}_h$ is a slowly varying amplitude function, its value is nearly unchanged from x_j to x_j+u_j. We simplify Eq. (22) to

$$\begin{aligned}\Phi_{z'}(\varphi) &\approx \frac{k\Delta\chi}{4\pi\cos\theta}\sum_h\sum_j(-1)^j\bar{E}_h(x_j,z') \\ &\quad\times\frac{\exp[i(h\upsilon-\varphi)(x_j+u_j)^2] - \exp[i(h\upsilon-\varphi)x_j^2]}{h\upsilon-\varphi},\end{aligned}$$

$$\upsilon = \pi/\lambda f. \tag{23}$$

Although $\Phi_{z'}$ is a continuously varying function, due to the overall periodicity of $\delta\chi$ in terms of X its value concentrates on separated spots,

$$\varphi = l\upsilon, \quad l = 0, \pm 1, \pm 2\ldots.$$

Hence we can write

$$\begin{aligned}s_{z'}(\mathbf{r}) &= \exp(i\mathbf{k_0}\cdot\mathbf{r})\sum_l\exp(il\upsilon x^2) \\ &\quad\times\int_{-\upsilon/2}^{\upsilon/2}\Phi_{z'}(l\upsilon+\Delta\varphi)\exp(i\Delta\varphi X)d\Delta\varphi \\ &= \exp(i\mathbf{k_0}\cdot\mathbf{r})\sum_l A_{z',l}(x)\exp[i\phi_l(x)],\end{aligned}$$

$$A_{z',l}(x) = \int_{-\upsilon/2}^{\upsilon/2}\Phi_{z'}(l\upsilon+\Delta\varphi)\exp(i\Delta\varphi X)d\Delta\varphi. \tag{24}$$

Each wave component in the source fluctuating wave, $A_{z',l}(x)\exp[i\mathbf{k_0}\cdot\mathbf{r}+i\phi_l(x)]$, propagates through the rest of the MLL with flat interfaces and gives rise to a wave field on the exit surface,

$$\tilde{E}_{z',l}(\mathbf{r_e}) = \sum_m \tilde{E}_{z',l,m}(\mathbf{r_e})\exp[i\mathbf{k_0}\cdot\mathbf{r_e} + i\phi_m(x)]. \tag{25}$$

In Eq. (25) $\tilde{E}_{z',l}(\mathbf{r})$ is the solution to

$$\nabla^2\tilde{E}_{z',l}(\mathbf{r}) + k^2[1+\bar{\chi}(\mathbf{r})]\tilde{E}_{z',l}(\mathbf{r}) = 0, \tag{26}$$

with the boundary conditions

$$\tilde{E}_{z',l,l}(x,z') = A_{z',l}(x) \text{ and } \tilde{E}_{z',l,m\neq l}(x,z') = 0.$$

Similarly, one can solve $\tilde{E}_{z',l}(\mathbf{r})$ using the technique developed in Ref. 14. From Eq. (8) one can see

$$\begin{aligned}&\int\int_\Omega p_{z'}(\mathbf{r};\mathbf{r_e})s_{z'}(\mathbf{r})dxdy \\ &= \sum_l\tilde{E}_{z',l}(\mathbf{r_e}) = \sum_l\sum_m\tilde{E}_{z',l,m}(\mathbf{r_e})\exp[i\mathbf{k_0}\cdot\mathbf{r_e}+i\phi_m(x)].\end{aligned}$$

To elucidate the excitation of the fluctuating wave on the exit surface, the sequential scattering processes are depicted in Fig. 2. Consequently one arrives at

$$\delta E(\mathbf{r_e}) = \sum_m \delta E_m(\mathbf{r_e})\exp[i\mathbf{k_0}\cdot\mathbf{r_e}+i\phi_m(x)],$$

$$\delta E_m(\mathbf{r_e}) = \int_0^t\sum_l\tilde{E}_{z',l,m}(\mathbf{r_e})dz'. \tag{27}$$

Further simplifications are possible. In many cases it is sufficient to consider only the zeroth- and the negative first-order diffractions (two-beam approximation; $h,l,m=0,-1$). Equation (27) is then reduced to

$$\delta E_{-1}(\mathbf{r_e}) = \int_0^t[\tilde{E}_{z',0,-1}(\mathbf{r_e}) + \tilde{E}_{z',-1,-1}(\mathbf{r_e})]dz',$$

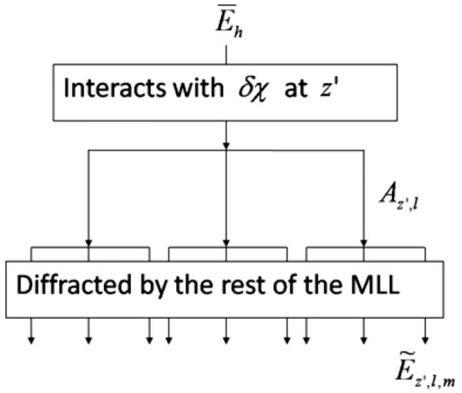

FIG. 2. The sequence of scattering processes. The hth wave component of the reference wave excites the lth wave component of the source fluctuating wave at z', which is then diffracted by the rest of the MLL with flat interfaces, resulting in the mth wave component of the fluctuating wave on the exit surface.

$$\delta E_0(\mathbf{r_e}) = \int_0^t [\tilde{E}_{z',0,0}(\mathbf{r_e}) + \tilde{E}_{z',-1,0}(\mathbf{r_e})]dz'. \tag{28}$$

Equation (28) describes two excitation modes of the fluctuating wave:

(1) The zeroth-order component in the reference wave, a plane wave, interacts with the roughness within a thin slice at z' and strongly excites the negative first-order component of the source fluctuating wave, which is diffracted dynamically by the rest of the MLL with flat interfaces, resulting in a fluctuating wave with both the zeroth- and the negative first-order components on the exit surface.

(2) The zeroth-order component in the source fluctuating wave is strongly excited by the negative first-order component in the reference wave, and it also leads to a fluctuating wave with both the zeroth- and the negative first-order components on the exit surface as it propagates through the rest of the MLL. Higher-order perturbations corresponding to the interaction of the fluctuating wave with roughness are neglected. Therefore this formalism is equivalent to the first-order DWBA as was stated earlier.

It is evident that the first-order DWBA becomes invalid when the fluctuating wave is comparable to the reference wave. Since one expects that the actual diffracted wave will deviate from the reference wave significantly as interface roughness increases, high-order corrections are necessary in this study. In other words, the interaction between the fluctuating wave and roughness must be taken into account. The reference wave needs to be updated during the calculation to reflect the change in the actual wave field. Hence a different reference wave should be used,

$$\bar{E}'_h(x_j,z') = \bar{E}_h(x_j,z') + \delta E_h(x_j,z'), \quad h = 0,-1. \tag{29}$$

Because the diffraction occurs in the transmission geometry, the fluctuating wave propagating to the front surface of a slice is a superposition of fluctuating waves generated in all preceding ones, and on its back surface the newly excited fluctuating wave only affects the wave field in the subsequent region. This forward diffraction scenario indicates that

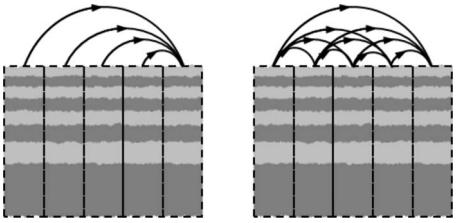

FIG. 3. Calculation schemes of the first-order DWBA (left) and DWBA with high-order corrections (right). The right graph shows that the reference wave at a position z' is updated every time when the fluctuating wave generated in a preceding slice at z'' propagates to it.

if we start the calculation from the first slice at $z'=0$ at which $\bar{E}'_h$ is known, the updated reference wave in the second slice, which is only affected by the fluctuating wave generated in the first slice, corresponds to the actual diffracted wave at this position. Using this, we can calculate the fluctuating wave excited by the updated reference wave in the second slice and update the reference wave in all subsequent slices. This process is repeated until the last slice at $z'=t$ is reached and a solution to the original wave equation is obtained. In such a way scattering processes 3 and 4 are taken into account and one has

$$\delta E_{-1}(\mathbf{r}) = \int_0^{z'} [\tilde{E}_{z'',0,-1}(\mathbf{r}) + \tilde{E}_{z'',-1,-1}(\mathbf{r})]dz'',$$

$$\delta E_0(\mathbf{r}) = \int_0^{z'} [\tilde{E}_{z'',0,0}(\mathbf{r}) + \tilde{E}_{z'',-1,0}(\mathbf{r})]dz'', \quad \mathbf{r} = (x,z'), \tag{30}$$

where $\tilde{E}_{z'',l,m}$ $(l,m=0,-1)$ is defined in Eqs. (25) and (26) and $A_{z'',l}$ is defined in Eq. (24) with the updated reference wave defined in Eq. (29). To clarify the difference between Eqs. (28) and (30), calculation schemes corresponding to the first-order DWBA and DWBA with high-order corrections are illustrated in Fig. 3.

Behind the MLL, the wave field at a point $\mathbf{r_f}=(\tau,t+L)$ around the first-order focus can be calculated by Huygens-Fresnel principle. Employing the stationary phase method to integrate out the y dimension, one arrives at

$$E(\mathbf{r_f}) \approx -\frac{i\exp(i\pi/4 + ikL + ik_{0z}t)}{\sqrt{L\lambda}} \int \bar{E}'_{-1}(\mathbf{r_e})\exp[i\psi(x)]dx,$$

$$\psi(x) = k(\sin\theta - \tau/L)x + kx^2(1/2L - 1/2f), \tag{31}$$

where f is the focal length. In this calculation a Fresnel approximation is applied. The prefactor outside the integral is of no importance in this study and will be dropped in the following discussion.

For a known height function u_j of the jth interface, the resultant aberration on the focus can be evaluated directly from Eq. (31). For stochastic roughness, however, a configurational average has to be carried out. For uncorrelated roughness one has

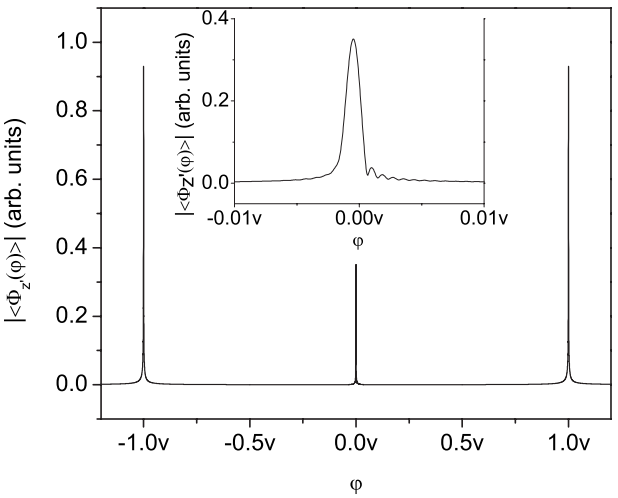

FIG. 4. The averaged spectrum of the source fluctuating wave after performing a Fourier transform with respect to X, showing narrow peaks centered at lv. The inset shows the peak at origin.

$$\langle |E(\mathbf{r}_\mathbf{f})|^2 \rangle = \left| \int [\bar{E}_{-1}(\mathbf{r}_\mathbf{e}) + \langle \delta E_{-1}(\mathbf{r}_\mathbf{e}) \rangle] \exp[i\psi(x)] dx \right|^2. \tag{32}$$

Roughness correlation is beyond the scope of this paper and is not considered here. Because the diffraction system described by Eq. (26) is linear, averaging on the fluctuating wave on the exit surface is equivalent to averaging on the source fluctuating wave or, in other words, on $A_{z',l}$. Based on Eq. (24) we first need to evaluate the average of the spectrum function $\Phi_{z'}$. For a Gaussian random variable u_j with rms roughness σ_j and zero mean, it is easy to derive

$$\langle \Phi_{z'} \rangle \approx \frac{\Delta\chi k}{4\pi \cos\theta} \sum_h \sum_j \bar{E}'_h(x_j, z')(-1)^{j(1+|h-l|)} \times \frac{\exp(-i\Delta\varphi x_j^2)}{(h-l)v - \Delta\varphi} \times [\exp(-\{[(h-l)v - \Delta\varphi]2x_j\sigma_j\}^2/2) - 1]. \tag{33}$$

In Eq. (33) the following relationship and approximations are utilized:

$$\exp[i(h-l)vx_j^2] = (-1)^{j|h-l|}, \quad \exp[i(h-l)vu_j^2] \approx 1, \quad \text{and} \quad \exp(-i\Delta\varphi u_j^2) \approx 1.$$

These approximations are valid for a roughness of no more than a few nanometers. In Fig. 4 we plot the averaged spectrum, assuming σ_j varies slowly over interfaces. As can be seen from the plot, $\langle \Phi_{z'} \rangle$ has an appreciable value only within a region much smaller than v. Therefore the integral in Eq. (24) is mainly contributed from this region and one can treat $\Delta\varphi$ as zero in Eq. (33) except for the quadratic phase term, which yields

$$\langle A_{z',l}(x) \rangle \approx \frac{\Delta\chi k}{4\pi \cos\theta} \sum_h \sum_j \bar{E}'_h(x_j, z')(-1)^{j(1+|h-l|)} \times \int_{-v/2}^{v/2} d\Delta\varphi \frac{\exp[i\Delta\varphi(x^2 - x_j^2)]}{(h-l)v} \times (\exp\{-[(h-l)v2x_ju_j]^2/2\} - 1). \tag{34}$$

With the two-beam approximation, one arrives at

$$\langle A_{z',0}(x) \rangle = -\frac{\Delta\chi k}{2\pi \cos\theta} \sum_j \bar{E}'_{-1}(x_j, z') \frac{\sin[(x^2 - x_j^2)v/2]}{v(x^2 - x_j^2)} \times \{\exp[-(2vx_j\sigma_j)^2/2] - 1\},$$

$$\langle A_{z',-1}(x) \rangle = \frac{\Delta\chi k}{2\pi \cos\theta} \sum_j \bar{E}'_0(x_j, z') \frac{\sin[(x^2 - x_j^2)v/2]}{v(x^2 - x_j^2)} \times \{\exp[-(2vx_j\sigma_j)^2/2] - 1\}. \tag{35}$$

Due to the property of the Sinc function, only a few terms with x_j very close to x contribute significantly to the value of $\langle A_{z',l}(x) \rangle$. If σ_j changes very slightly from one interface to the other, we can treat both $\bar{E}'_l(x_j, z')$ and $\exp[-(2vx_j\sigma_j)^2/2]$ as constants over a few interfaces near x. In addition, for x not close to the first or the last interface, the following approximation is valid:

$$\sum_j \frac{\sin[(x^2 - x_j^2)v/2]}{v(x^2 - x_j^2)} \approx 1.$$

As a result, Eq. (35) can be expressed into a fairly simple form,

$$\langle A_{z',0}(x) \rangle \approx -\frac{\Delta\chi k}{2\pi \cos\theta} \bar{E}'_{-1}(x, z')(\exp\{-[2vx\sigma(x)]^2/2\} - 1),$$

$$\langle A_{z',-1}(x) \rangle \approx \frac{\Delta\chi k}{2\pi \cos\theta} \bar{E}'_0(x, z')(\exp\{-[2vx\sigma(x)]^2/2\} - 1), \tag{36}$$

where $\sigma(x)$ is a continuously varying function with $\sigma(x_j) = \sigma_j$. One may recognize

$$2vx = \frac{2\pi x}{\lambda f} = \frac{2\pi}{2\Delta x} = \rho(x),$$

where $\rho(x)$ is the modulus of the local reciprocal-lattice vector of the negative first order. Therefore it is more meaningful to write the last term in Eq. (36) as

$$\exp[-(\rho\sigma)^2/2] - 1 = \exp[-(\pi\sigma/\Delta x)^2/2] - 1. \tag{37}$$

This expression indicates that the magnitude of the source fluctuating wave is determined by the σ to Δx ratio.

III. NUMERICAL SIMULATIONS

A. Known height function

For a known height profile, it is possible to calculate the diffracted wave directly from the rigorous formalism.[14] This

provides the "experimental data" in a computer experiment to check the correctness and validity of the DWBA modeling approach developed in this paper. Let us consider an MLL with flat zones and with the parameters $f=2.6$ mm, $t=10$ μm, and $x_{\max}=16.5$ μm, and an outmost zone width of 5 nm. It consists of thousands of alternating layers of WSi_2 and Si. A plane wave at energy of 19.5 keV illuminates the MLL at a tilting angle of 0.15°. It is assumed that all interfaces have the same height function

$$u_j = u = u_0 \exp[-(z - t/2)^2]. \tag{38}$$

That is, each zone is displaced equally by a small distance which reaches the maximum value of u_0 in the middle. The susceptibility function of this MLL is then written as

$$\chi = \chi_0 + \sum_{h,h\neq 0} \chi_h \exp[i\phi_h(x-u)] = \chi_0 + \sum_{h,h\neq 0} \chi_h(x,z)\exp[i\phi_h(x)], \tag{39}$$

where

$$\chi_0 = (\chi_A + \chi_B)/2,$$

$$\chi_h(x,z) = \frac{\chi_A - \chi_B}{2ih\pi}[1-(-1)^{|h|}]\exp\left[i\frac{h\pi}{\lambda f}(-xu+u^2)\right]. \tag{40}$$

Now the coefficient of the hth ($h\neq 0$) pseudo-Fourier component is no longer a constant but is position dependent. Substituting this expression into Eq. (16) of Ref. 14, one can solve diffracted waves of different orders as well as the change in the wave field, δE, associated with this small displacement. For comparison, δE is also calculated from the first-order DWBA [Eq. (28)] and DWBA with high-order corrections [Eq. (30)]. Two cases, corresponding to $u_0=1$ and 3 nm, are studied and the results are plotted in Fig. 5. In the case of $u_0=1$ nm, the negative first order of the fluctuating wave has weak amplitude. It is found that the result obtained from the first order DWBA with the two-beam approximation agrees with that obtained from the rigorous calculation very well, except for positions around $x=6$ μm. The difference observed around this position is attributed to the strong excitation of higher orders of diffraction. A further study shows that at this position the intensity of the negative second order is not negligible due to a strong coupling with the negative first order, which is a purely dynamical effect. On the other hand, the two-beam approximation is sufficient in the outer region where only the zeroth- and the negative first-order waves are very strong.

When u_0 is increased to 3 nm, however, a considerable difference is observed between the first-order DWBA and the rigorous calculation. This is because the requirement for the validity of the first-order DWBA, $|\delta E| \ll |E|$, is not satisfied any more. As can be seen in the inset of Fig. 5, the value of $|\delta E_{-1}/\bar{E}_{-1}|$ exceeds 0.1 in most regions and reaches almost 0.5 in the outer part. The fluctuating wave can no longer be treated as a small perturbation, and high-order corrections, which take into account the interaction of the fluctuating

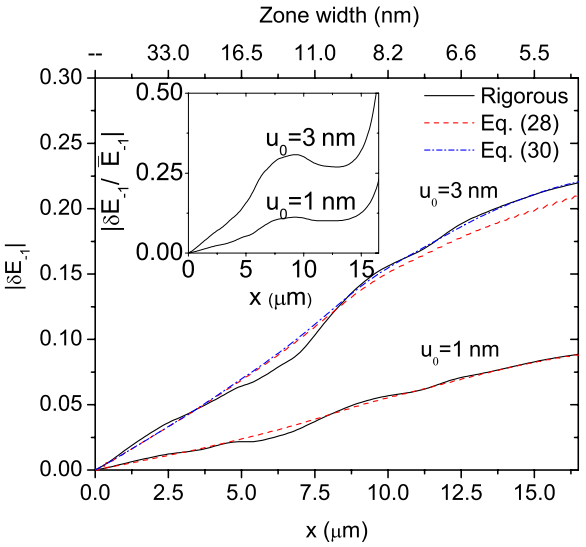

FIG. 5. (Color online) The amplitude of the negative first-order component of the fluctuating wave on the exit surface due to a height function, $u=u_0\exp[-(z-t/2)^2]$. Results are calculated from the rigorous formalism (solid line), the first-order DWBA [Eq. (28); dashed line], and DWBA with high-order corrections [Eq. (30); dash-dotted line]. The inset shows the $|\delta E_{-1}/\bar{E}_{-1}|$ ratio.

wave with roughness, are required. As was indicated earlier, Eq. (30) has to be employed. The result obtained from Eq. (30) shows good agreement with the rigorous calculation again. Only in the inner part where other orders of diffraction are not negligible there is a slight difference observed.

To check the validity of Eq. (30) in the case of a very strong perturbation, we consider a second example where wavy interfaces are present,

$$u_j = u = u_0 \sin(z - t/2). \tag{41}$$

In the extreme case of $u_0=5$ nm, the variation in the local diffraction intensity of the negative first order on the exit surface is plotted in Fig. 6 using the rigorous formalism, Eqs. (28) and (30). As can be seen from the simulation, the presence of a wavy interface leads to a quick decrease in the local diffraction intensity to nearly zero in the outer region of the MLL, and it is certainly beyond the range of validity of the first-order DWBA. As expected, Eq. (28) fails to produce the correct result. On the other hand, Eq. (30) is capable of predicting precisely the variation in the local diffraction intensity in the outer region even in this extreme case. The small difference observed in the inner part as compared to the rigorous calculation is again a result of the two-beam approximation. It is evident that after taking into account high-order corrections the DWBA model developed here is also capable of dealing with a very strong perturbation. In what follows and unless otherwise specified, the DWBA with high-order corrections and the two-beam approximation [Eq. (30)] will be employed for all theoretical simulations.

B. Stochastic roughness without correlation

For stochastic roughness, the average over ensembles for all possible height functions has to be evaluated. For simplic-

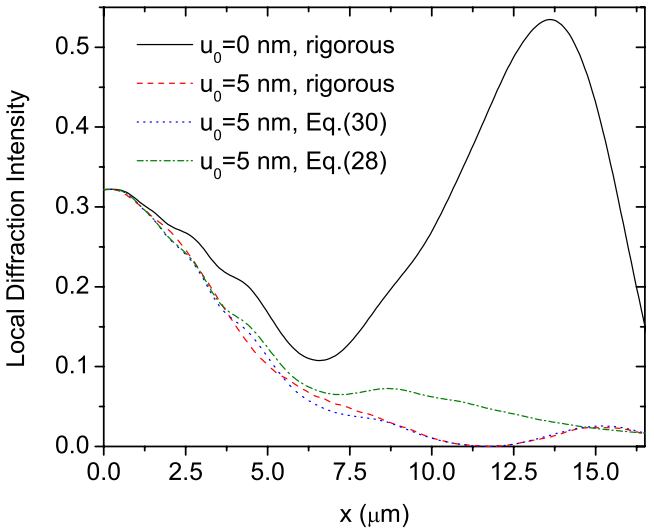

FIG. 6. (Color online) Variation in the local diffraction intensity of the negative first order for wavy interfaces. Results are calculated from the rigorous formalism, the first-order DWBA [Eq. (28)], and DWBA with high-order corrections [Eq. (30)].

ity it is assumed that all interfaces possess roughness profiles following the same Gaussian normal distribution with rms roughness of σ and zero mean. That is, the mean interface position does not deviate from the desired value calculated from the zone plate law. The MLL studied has the same parameters as specified in Sec. IIA. Figure 7 shows the local diffraction intensity of the negative first order when $\sigma=0$ (no roughness), 1, 2, and 3 nm. As can be seen from simulation results, interface roughness causes a decrease in the local diffraction intensity and the qualitative amount of decrease is proportional to σ. It is seen that in all cases the local diffraction intensity of the inner part is affected much less significantly than that of the outer part, which implies that the attenuation factor $\xi(x,\sigma)$ should be a function of $\sigma/\Delta x$, where Δx is the local zone width at x. This is also suggested by the expression of $A_{z',l}$ in Eqs. (36) and (37). In the inset of Fig. 7, attenuation factors at positions with $\Delta x=10$, 6, and 5 nm are plotted in terms of the $\sigma/\Delta x$ ratio. In this particular case, they follow almost the same curve which can be fitted by a function $\xi(x,\sigma)=\exp[-b(\sigma/\Delta x)^c]$, with $b=9.76$ and $c=2.23$. Using this function one can predict that when $\sigma/\Delta x$ is smaller than 0.1 the attenuation factor is about 0.94; thus, one may consider that the local diffraction intensity is unaffected. When $\sigma/\Delta x$ is increased to 0.5 it drops down to 0.12; a very significant decrease in the local diffraction intensity will be observed. For the total focusing efficiency, which is defined as the integrated local diffraction intensity normalized by the integrated incoming x-ray intensity, it may be convenient to plot its change in terms of the $\sigma/\Delta x_{\min}$ ratio. The attenuation factor for the total focusing efficiency is plotted in Fig. 8. We observe a less than 5% decrease in the total focusing efficiency when σ is smaller than 10% of the outmost zone width, while an almost 50% decrease in the total focusing efficiency is observed as σ reaches 50% of the outmost zone width.

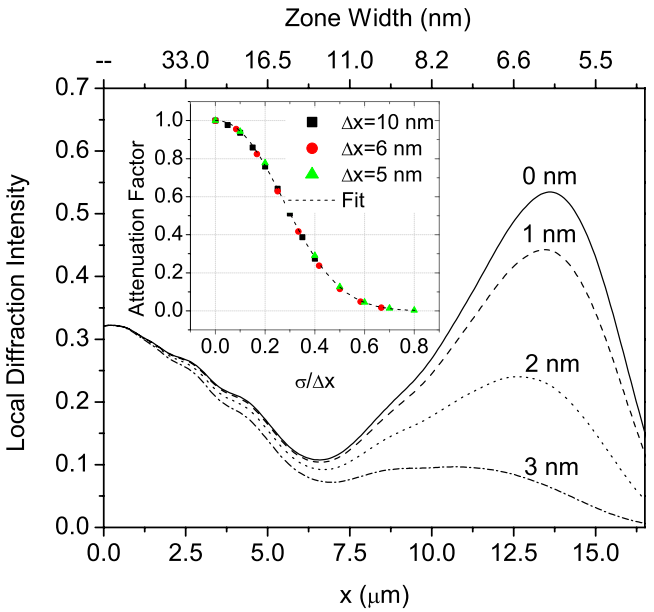

FIG. 7. (Color online) Variation in the local diffraction intensity of the negative first order on the exit surface at different σ values. The inset shows the change in attenuation factor at different locations as a function of $\sigma/\Delta x$.

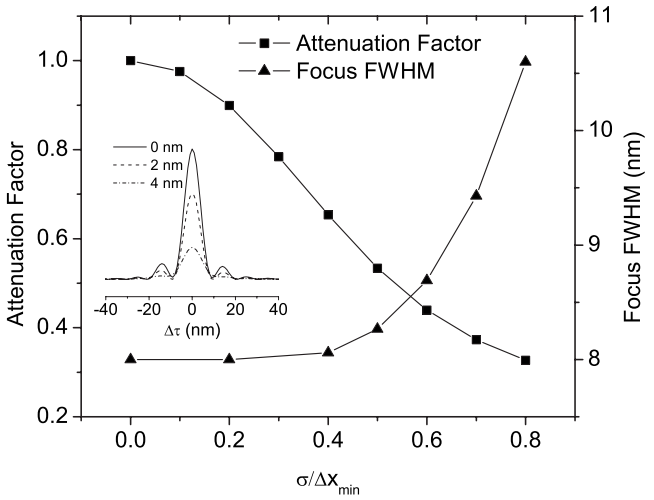

FIG. 8. The attenuation of the total focusing efficiency and the focus peak half-width as a function of the $\sigma/\Delta x_{\min}$ ratio. The inset shows focus profiles when $\sigma=0$, 2, and 4 nm.

In addition to the attenuation factor, focus profiles at $\sigma=0$, 2, and 4 nm (inset) and the change in the full width at half maximum (FWHM) of the focal peak are also plotted in Fig. 8. We can see that the focus size increases noticeably as the value of $\sigma/\Delta x_{\min}$ approaches 1. This is because the electron density contrast in the outer region of the MLL is smeared out and the local diffraction intensity is attenuated so significantly that this region does not contribute to focusing anymore (see Fig. 7). When the $\sigma/\Delta x_{\min}$ ratio ranges from 0 to 0.5, the FWHM of the focal peak only changes slowly from 8 to 8.3 nm and this change may be considered negligible. When this ratio is greater than 0.5, the focal peak width increases quickly to a noticeable level.

Based on these simulations, we may conclude that if σ is smaller than 10% of the outmost zone width of an MLL, the

effect of interface roughness is negligible in terms of both efficiency and the focal size. Before σ reaches half of the outmost zone width, the MLL may suffer a significant loss in the focusing efficiency while its focal size is not noticeably broadened. As σ increases to above half of the outmost zone width, the broadening effect on the focal size becomes appreciable.

However, due to the complexity of the dynamical diffraction, neither for the decrease of the focusing efficiency nor for the broadening of the focus can an analytical expression be derived. Their functional forms may change from case to case. A numerical simulation has to be carried out in each case. One particularly important case is the wedged multilayer Laue lens (wMLL) with 1-nm outmost zone width, which is the candidate optic for achieving 1-nm focusing at the planned National Synchrotron Light Source II.[26] A conceptual demonstration of wMLLs by sputtering-deposition techniques has been reported.[27] In practice it is not possible to control the interface roughness within 0.1 nm. Therefore the roughness problem is inevitable and its effect has to be evaluated.

The wMLL considered here has the parameters $f=1$ mm, $t=16$ μm, and $x_{\max}=31$ μm and 1-nm outmost zone width. It is illuminated by a plane wave at 19.5 keV in normal direction ($\theta=0$). Again, only half of the wMLL on the positive x axis is considered. The jth interface of the wMLL is determined by the zone plate law,

$$x_j(z) = a(z)\sqrt{j\lambda f + j^2\lambda^2/4}, \quad a(z) = 1 - z/2f, \tag{42}$$

which is also a function of depth z because of the wedged shape of the zone. With a few modifications all equations derived above for flat zones can be applied to wMLLs,

$$\phi_h(x,z) = hk\{\sqrt{[x/a(z)]^2 + f^2} - f\},$$

$$\langle A_{z',0}(x)\rangle = -\frac{\Delta\chi k}{2\pi}\bar{E}'_{-1}(x,z')\{\exp[-(\rho_x\sigma)^2/2] - 1\},$$

$$\langle A_{z',-1}(x)\rangle = \frac{\Delta\chi k}{2\pi}\bar{E}'_{0}(x,z')\{\exp[-(\rho_x\sigma)^2/2] - 1\},$$

$$\rho_x = \left|\frac{\partial\phi_{\pm1}}{\partial x}\right| = \frac{2\pi[x/a(z')]}{a(z')\lambda\sqrt{[x/a(z')]^2 + f^2}}. \tag{43}$$

Figure 9 shows the local diffraction intensities of the negative first order with rms roughnesses equal to 0, 0.3, and 0.5 nm. In the absence of roughness, the local diffraction intensity curve may be divided into three sections. In section I where the zone width is larger than 20 nm and the MLL behaves more like a thin grating, low diffraction intensity of about 0.13 is observed, in agreement with the number calculated from the geometrical-optical theory for a zone plate with $t=16$ μm. In section II where the zone width is below 20 nm but is larger than 2 nm, the diffraction intensity is boosted sharply to about 0.7 because of the strong dynamical diffraction effect, and it only varies slightly in this section. When section III is reached, the local diffraction intensity decreases gradually to about 0.26 since the wMLL is only an approximation to the ideal structure for focusing x rays.

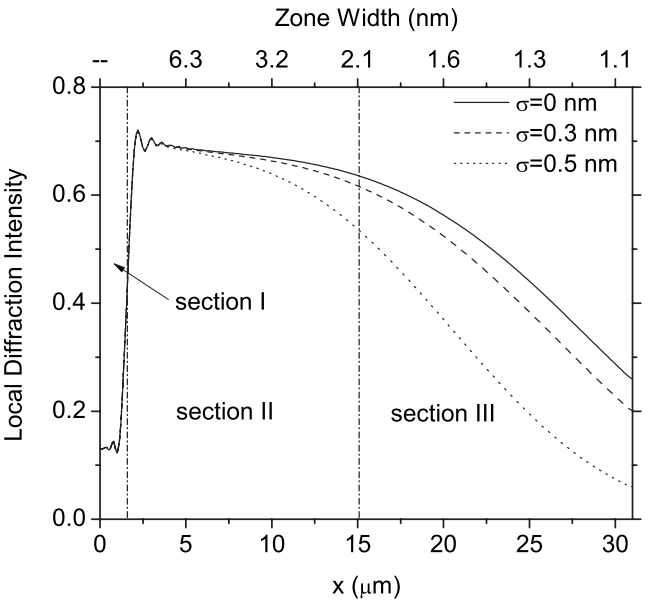

FIG. 9. Variation in the local diffraction intensity of the negative first order of a wedged MLL with 1-nm outmost zone width for σ values of 0, 0.3, and 0.5 nm.

When interface roughness is present, for $\sigma=0.3$ and 0.5 nm the local diffraction intensity in section I is unchanged because the value of $\sigma/\Delta x$ is smaller than 0.1. In section II, the attenuation starts to be appreciable around $\Delta x=3$ nm for $\sigma=0.3$ nm and $\Delta x=5$ nm for $\sigma=0.5$ nm, in agreement with the conclusions drawn previously for MLLs with flat zones. As the $\sigma/\Delta x$ ratio goes up further in section III, the attenuation effect due to roughness becomes much more pronounced. For instance, for $\sigma=0.5$ nm at $x=31$ μm the local diffraction intensity drops from 0.26 to 0.06, a more than fourfold reduction. Unlike the case of MLLs with flat zones, a simple attenuation factor $\xi(x,\sigma)$ that works at all roughness levels is not observed. Although an approximation of ξ can be fitted by a similar function, $\xi=\exp[-b(\sigma/\Delta x)^c]$, it is found that b and c vary with σ.

Figure 10 shows the attenuation of the total focusing efficiency as a function of the $\sigma/\Delta x_{\min}$ ratio. Before this ratio reaches 0.3, it can be seen that the attenuation is almost negligible. When σ increases to half of the outmost zone width, the total focusing efficiency is reduced by about 22%. The focal broadening effect due to roughness is also studied in this case. For $\sigma=0$ and 0.3 nm, a focal peak with 1.80 nm FWHM is observed. When σ is increased to 0.5 nm, the focal peak width is increased slightly to about 1.95 nm due to the fact that the diffraction intensity in the outmost region drops down to nearly zero. This part of the lens does not contribute to focusing effectively. We can see that the focal broadening effect becomes more pronounced as σ increases further (see Fig. 10), since a larger fraction of the lens will have nearly zero diffraction intensity. Thus, the rms roughness for this wMLL has to be controlled within 0.5 nm in order not to see an appreciable broadening of the focus.

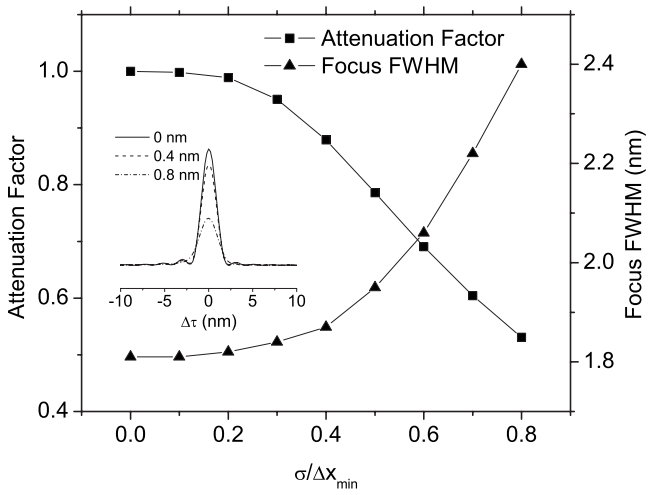

FIG. 10. The attenuation of the total focusing efficiency and the focal peak half-width as a function of the $\sigma/\Delta x_{\min}$ ratio for the 1-nm wMLL. The inset shows focus profiles when σ=0, 0.4, and 0.8 nm.

IV. CONNECTION TO INTERDIFFUSION PROBLEM

One sometimes needs to consider the interdiffusion problem, i.e., the susceptibility function χ varies gradually across the zone boundary. As a result the MLL has graded interfaces instead of sharp ones. An interesting question arises as to whether one can equate a rough interface to a graded one. Of course, in the case of a graded interface there is no diffuse scattering that is related to roughness correlation. The discussion here is restricted to uncorrelated roughness. We have shown that averaging on the fluctuating wave after a segment was equivalent to averaging on the source fluctuating wave generated in the upfront thin slice, which yields [from Eq. (14)]

$$\langle s_{z'}(\mathbf{r})\rangle = \frac{ik}{2\cos\theta}\langle\delta\chi(\mathbf{r})\rangle\bar{E}(\mathbf{r}), \quad \mathbf{r}=(x,z'). \tag{44}$$

Hence one can take the average on $\delta\chi$ first and then calculate the perturbation. If we take the susceptibility function

$$\chi = \bar{\chi} + \langle\delta\chi\rangle \tag{45}$$

for an MLL with graded interfaces (for simplicity flat zones are assumed), the diffracted wave field within it should be no different from that in an MLL with equivalent rough interfaces. For a Gaussian random variable u_j, the mean susceptibility function is

$$\langle\chi\rangle = \bar{\chi} + 0.5\Delta\chi\sum_j (-1)^j\left[\mathrm{sgn}(x-x_j) - \mathrm{erf}\left(\frac{x-x_j}{\sqrt{2}\sigma_j}\right)\right], \tag{46}$$

where erf is the error function. Using the same technique of deriving $A_{z',l}(x)$, one can expand $\langle\chi\rangle$ in Eq. (46) into a pseudo-Fourier series,

$$\langle\chi\rangle = \sum_h \chi_h(x)\exp[i\phi_h(x)],$$

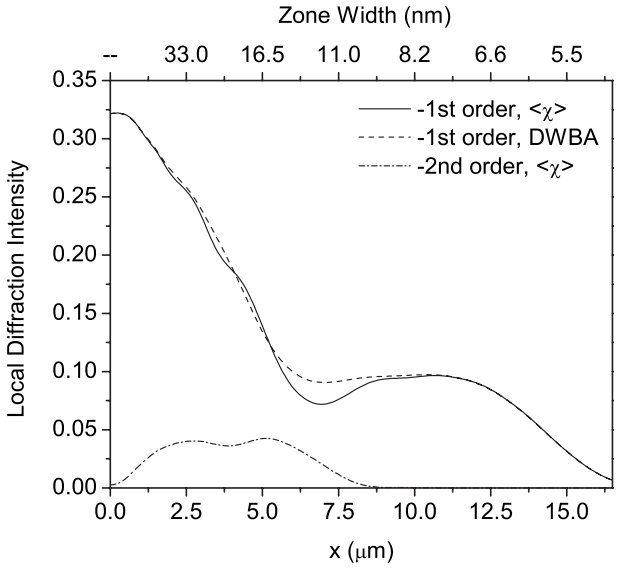

FIG. 11. Variation in the local diffraction intensity of the negative first order calculated using a mean χ and the DWBA. The negative second order is also plotted.

$$\chi_0 \approx (\chi_A + \chi_B)/2,$$

$$\chi_{h\neq 0}(x) \approx \frac{\chi_A - \chi_B}{2ih\pi}[1-(-1)^{|h|}]\exp[-(2hvx\sigma)^2/2], \quad \sigma_j = \sigma, \tag{47}$$

which are simply the constant pseudo-Fourier coefficients for MLLs with flat interfaces multiplied by a roughness factor, $\exp(-M_h)=\exp[-(2hvx\sigma)^2/2]$, similar to the Debye-Waller factor. We may express this factor in a more meaningful form, $\exp(-M_h)=\exp(-\rho_h^2\sigma^2/2)$, where ρ_h is the modulus of the hth local reciprocal-lattice vector. If this is extended to MLLs with arbitrary zone profiles, the roughness factor is written as

$$\exp(-M_h) = \langle\exp(i\boldsymbol{\rho}_\mathbf{h}\cdot\mathbf{u})\rangle, \quad \boldsymbol{\rho}_\mathbf{h} = \nabla\phi_h, \tag{48}$$

where $\mathbf{u}$ is the random displacement vector of the interface.

Substituting Eq. (47) into Eq. (16) of Ref. 14, one can solve the problem easily. In Fig. 11 the result calculated by using a mean susceptibility function is compared with that obtained from DWBA for σ=3 nm. The MLL parameters are the same as those used in Fig. 7. Very good agreement is observed in the region with zone width smaller than 10 nm, indicating that we can equate interface roughness to interdiffusion. The difference observed in the inner part between the two models is due to a strong excitation of the negative second-order diffraction which is also shown in the figure. We note that using 1D coupled wave theory, Schneider[16] previously demonstrated the similarity of the influence of roughness and interdiffusion on a zone plate.

One shall note that the equivalence of interface roughness and interdiffusion is a result of following observations:

(1) The interface roughness is completely uncorrelated.

(2) The unperturbed system is linear, so that averaging on the resultant fluctuating wave on the exit surface of the MLL is equivalent to averaging on the source fluctuating wave.

(3) The source fluctuating wave can be simply written as a product of the fluctuation of the susceptibility function and the reference wave [Eq. (14)], so that averaging on the source fluctuating wave is equivalent to averaging on $\delta\chi$. In the x-ray domain, χ is so small that the approximations made in obtaining Eq. (14) is usually valid. However, if the wave field far away from the focus is of interest, we have $\mathbf{k} \neq \mathbf{k_0}$ and Eq. (14) may not be valid.

(4) For strong perturbations an updated reference wave $\bar{E}'$ has to be used in the calculation. As was discussed in Sec. III, because of the transmission geometry the value of $\bar{E}'$ at z' is not affected by the value of $\delta\chi$ at the same position. Therefore averaging on the source fluctuating wave is still equivalent to averaging on $\delta\chi$ at z'. That is, if the source fluctuating wave is a function of $\delta\chi$, we have

$$\langle s_{z'}(\mathbf{r})\rangle = \langle F[\delta\chi(\mathbf{r})]\rangle = F(\langle\delta\chi(\mathbf{r})\rangle).$$

In the case where interface roughness can be treated in the same way as that for interdiffusion, an exact solution for the diffracted wave by using the roughness factor is obviously superior to the DWBA method. But one should be aware of the range of validity of all assumptions and approximations made in reaching Eqs. (47) and (48). On the other hand, the DWBA modeling allows a calculation of the diffuse scattering and is more general.

V. SUMMARY AND CONCLUSIONS

In summary, a modeling approach for x-ray scattering from multilayers with rough interfaces is developed. The principle of DWBA is employed in this model, but it is formulated from the physical picture of the scattering process, different from the conventional method that utilizes the time-inverted solution and is usually limited to Fraunhoffer diffraction and nonabsorptive samples. This approach extends DWBA into the regime of Fresnel diffraction and absorptive samples, well suited for the study of x-ray diffraction from MLL optics with rough interfaces. Moreover, high-order corrections are also taken into account so that it can deal with strong perturbations as well. This approach may find applicability in other cases where the conventional DWBA fails. The focusing performance of MLLs with flat and wedged zones and with various rms roughnesses is studied. Simulation results show that stochastic roughness results in a decrease in the local diffraction intensity. The theoretical study suggests that the rms roughness to zone width ratio can serve as a good parameter for quantifying the attenuation effect. It is found that when this ratio is below 0.1, the loss in the local diffraction intensity is usually negligible. In all cases studied, when the rms roughness is smaller than half of the outmost zone width of an MLL, no noticeable broadening effect on focus is observed although the reduction in the total focusing efficiency can be very considerable. We want to stress that all calculations here assume zero errors on the mean interface positions, so roughness does not introduce a big phase error into the wave field on the exit surface. The main effect of roughness is to attenuate the amplitude of the focusing wave.

The connection of interface roughness to interdiffusion is discussed. For uncorrelated roughness, it is found that a roughness factor similar to the Debye-Waller factor can be used to describe the adverse effect of roughness on MLLs focusing performance. In such cases, the pseudo-Fourier coefficients of the susceptibility function for an MLL have to be multiplied by this roughness factor.

Roughness correlations, which will result in an additional diffuse scattering term, are not discussed. One can deal with them in the framework of the DWBA model developed here, employing the diffracted wave solution obtained by using a mean susceptibility function as the reference wave.[28]

For MLLs that are made of WSi_2/Si multilayers and fabricated by sputtering-deposition techniques nowadays, *in situ* synchrotron studies have revealed that the noticeably rougher Si layer can be smoothened by the WSi_2 deposition afterward and interface roughness can be controlled below 0.5 nm.[29] According to the simulation shown in this paper, this level of roughness will cause a considerable loss in the total focusing efficiency, but will not broaden the focus size significantly. As a result roughness should not be a showstopper in practice for reaching 1 nm by MLL optics.

ACKNOWLEDGMENTS

The author would like to greatly acknowledge A. T. Macrander for stimulating discussions on this topic and also for a critical reading of the paper. This work was supported by the U.S. Department of Energy, Office of Science, Office of Basic Energy Sciences, under Contract No. DE-AC-02-98CH10886.

[1] H. C. Kang, J. Maser, G. B. Stephenson, C. Liu, R. Conley, A. T. Macrander, and S. Vogt, Phys. Rev. Lett. **96**, 127401 (2006).
[2] C. G. Schroer, O. Kurapova, J. Patommel, P. Boye, J. Feldkamp, B. Lengeler, M. Burghammer, C. Riekel, and L. Vincze, Appl. Phys. Lett. **87**, 124103 (2005).
[3] H. Mimura, H. Yumoto, S. Matsuyama, Y. Sano, K. Yamamura, Y. Mori, and M. Yabashi, Appl. Phys. Lett. **90**, 051903 (2007).
[4] Y. Suzuki, A. Takeuchi, H. Takano, and H. Takenaka, Jpn. J. Appl. Phys., Part 1 **44**, 1994 (2005).
[5] G.-C. Yin, Y.-F. Song, M.-T. Tang, F.-R. Chen, K. S. Liang, F. W. Duewer, M. Feser, W. Yun, and H.-P. D. Shieh, Appl. Phys. Lett. **89**, 221122 (2006).
[6] Y. S. Chu, J. M. Yi, F. De Carlo, Q. Shen, Wah-Keat Lee, H. J. Wu, C. L. Wang, J. Y. Wang, C. J. Liu, C. H. Wang, S. R. Wu, C. C. Chien, Y. Hwu, A. Tkachuk, W. Yun, M. Feser, K. S. Liang, C. S. Yang, J. H. Je, and G. Margaritondo, Appl. Phys. Lett. **92**, 103119 (2008).
[7] S. Matsuyama, H. Mimura, H. Yumoto, Y. Sano, K. Yamamura,

and M. Yabashi, Rev. Sci. Instrum. **77**, 103102 (2006).
[8] C. Bergemann, H. Keymeulen, and J. F. van der Veen, Phys. Rev. Lett. **91**, 204801 (2003).
[9] K. Evans-Lutterodt, J. Ablett, A. Stein, C.-C. Kao, D. Tennant, F. Klemens, A. Taylor, C. Jacobsen, P. Gammel, H. Huggins, G. Bogart, S. Ustin, and L. Ocola, Opt. Express **11**, 919 (2003).
[10] C. G. Schroer and B. Lengeler, Phys. Rev. Lett. **94**, 054802 (2005).
[11] J. Maser, G. B. Stephenson, S. Vogt, Y. Wenbing, A. Macrander, H. C. Kang, L. Chian, and R. Conley, Proc. SPIE **5539**, 185 (2004).
[12] C. Liu, R. Conley, A. T. Macrander, J. Maser, H. C. Kang, M. A. Zurbuchen, and G. B. Stephenson, J. Appl. Phys. **98**, 113519 (2005).
[13] H. C. Kang, H. Yan, R. P. Winarski, M. V. Holt, J. Maser, C. Liu, R. Conley, S. Vogt, A. T. Macrander, and G. B. Stephenson, Appl. Phys. Lett. **92**, 221114 (2008).
[14] H. F. Yan, J. Maser, A. Macrander, Q. Shen, S. Vogt, G. B. Stephenson, and H. C. Kang, Phys. Rev. B **76**, 115438 (2007).
[15] H. Yan, H. C. Kang, J. Maser, A. T. Macrander, C. M. Kewish, C. Liu, R. Conley, and G. B. Stephenson, Nucl. Instrum. Methods Phys. Res. A **582**, 126 (2007).
[16] G. Schneider, Appl. Phys. Lett. **73**, 599 (1998).
[17] A. N. Kurokhtin and A. V. Popov, J. Opt. Soc. Am. A **19**, 315 (2002).
[18] G. H. Vineyard, Phys. Rev. B **26**, 4146 (1982).
[19] S. K. Sinha, E. B. Sirota, S. Garoff, and H. B. Stanley, Phys. Rev. B **38**, 2297 (1988).
[20] V. Holy, J. Kubena, I. Ohlidal, K. Lischka, and W. Plotz, Phys. Rev. B **47**, 15896 (1993).
[21] V. Holy and T. Baumbach, Phys. Rev. B **49**, 10668 (1994).
[22] G. T. Baumbach, S. Tixier, U. Pietsch, and V. Holy, Phys. Rev. B **51**, 16848 (1995).
[23] V. M. Kaganer, S. A. Stepanov, and R. Kohler, Phys. Rev. B **52**, 16369 (1995).
[24] L. Rodberg and R. Thaler, *Introduction to the Quantum Theory of Scattering* (Academic, New York, 1967).
[25] S. V. Mytnichenko, Physica B **355**, 244 (2005).
[26] S. Dierker *et al.*, Brookhaven National Laboratory, NSLS-II Conceptual Design Report, 2006; http://www.bnl.gov/nsls2/project/CDR/.
[27] R. Conley, C. Liu, J. Qian, C. M. Kewish, A. T. Macrander, H. Yan, H. C. Kang, J. Maser, and G. B. Stephenson, Rev. Sci. Instrum. **79**, 053104 (2008).
[28] A. Sentenac and J. J. Greffet, J. Opt. Soc. Am. A Opt. Image Sci. Vis **15**, 528 (1998).
[29] Y.-P. Wang, H. Zhou, L. Zhou, R. L. Headrick, A. T. Macrander, and A. S. Ozcan, J. Appl. Phys. **101**, 023503 (2007).